Available online at www.sciencedirect.com
SCIENCE DIRECT®
Journal of Molecular Catalysis A: Chemical 232 (2005) 101–112
JOURNAL OF MOLECULAR CATALYSIS A: CHEMICAL
www.elsevier.com/locate/molcata

Effect of pre-treatment conditions on the performance of sulfided Ni–Mo/γ-Al_2O_3 catalysts for hydrogenation of linear aldehydes

Xueqin Wang, Umit S. Ozkan *

Department of Chemical Engineering, The Ohio State University, 140 W, 19th Avenue, Columbus, OH 43210, USA

Received 28 November 2004; received in revised form 19 January 2005; accepted 19 January 2005

Abstract

Effect of catalyst pre-treatment conditions on activity and selectivity of sulfided Ni–Mo/γ-Al_2O_3 catalysts in aldehyde hydrogenation reactions was studied. It appears that both of the sulfidation temperature and the post-sulfidation degassing temperatures can be effectively used to manipulate the surface density of anion vacancy sites and the hydroxyl and sulfhydryl sites over the sulfided Ni–Mo/γ-Al_2O_3 catalysts. Any changes in the surface density of these sites, in turn, can have significant effect on the activity and product distribution achieved over these catalysts in hydrogenation of linear aldehydes, hexanal and propanal. As established previously, NO and CO_2 can be used to probe the sites that promote the alcohol and heavy product formation reactions, respectively. The results obtained from XRD, XPS, DRIFTS, TPD and volumetric chemisorption measurements provide complementary information in establishing the correlations between the active sites and reaction performance.

Keywords: Aldehyde hydrogenation; Sulfided Ni–Mo catalysts; NO adsorption; CO_2 adsorption; Pyridine adsorption; DRIFTS; XPS

1. Introduction

Sulfided Ni–Mo and Co–Mo catalysts supported on Al_2O_3 are used extensively in many hydrotreating processes, including hydrodesulfurization (HDS), hydrodenitrogenation (HDN), hydrodeoxygenation (HDO) and hydrogenation (HYD). According to a widely accepted model by Topsøe et al., sulfidation of the oxide phases results in the formation of stacks of MoS_2 slabs over the support surface and the Ni and Co species are located primarily on the edges of these stacks [1–4]. Active site models based on these structures have been used to account for different product distributions observed in HDS, HDN, and HDO reactions [5–15]. Several of these studies have assigned the hydrogenation activity to coordinatively unsaturated sites (CUS), i.e., sulfur vacancies associated with Ni and Mo centers and the hydrogenolysis activity to Brønsted acid sites neighboring sulfhydryl groups. It was also proposed that reduced Ni–Mo/Al_2O_3 catalysts might exhibit similar activity where OH groups act in an analogous manner to SH groups and anion vacancies (CUS) can form during reduction process as well [16–18]. Although the relationships between different active sites, such as coordinatively unsaturated sites (CUS), Brønsted acid sites, SH and OH groups, over NiMoS and CoMoS catalysts and different reaction steps in HDS, HDN, and HDO reactions are studied extensively, similar correlations in aldehyde hydrogenation reactions have not been the focus of many studies.

Oxo process alcohols are a major class of organic chemicals [19]. The oxo process (i.e., hydroformylation) consists of reacting an olefin with carbon monoxide and hydrogen at elevated temperatures and pressures, in the presence of a suitable catalyst, to produce an aldehyde with a carbon number one higher than the starting olefin. Depending on the process conditions, the resulting products may be aldehydes, primary alcohols, or a mixture of the two. The product stream from the oxo process needs to be hydrogenated to convert the aldehydes to alcohols. Several different catalysts are used

* Corresponding author. Tel.: +1 614 292 6623; fax: +1 614 292 9615.
E-mail address: ozkan.1@osu.edu (U.S. Ozkan).

1381-1169/$ – see front matter © 2005 Elsevier B.V. All rights reserved.
doi:10.1016/j.molcata.2005.01.037

in industry to convert aldehydes to alcohols. Catalysts frequently used include copper chromite, molybdenum sulfide, nickel, and cobalt. Although copper chromite has excellent hydrogenation activity, it is also very sensitive to sulfur poisoning, making it difficult to use with sulfur containing feed streams. Sulfided Ni–Mo/Al_2O_3 catalysts provide excellent hydrogenation activity while showing a high tolerance to sulfur compounds. In our previous articles [20–22], we have reported on the catalytic performance of sulfided Ni–Mo/γ-Al_2O_3 catalysts in the hydrogenation of linear aldehydes to alcohols. The two primary reactions that are of most interest in these reaction schemes are the hydrogenation of the aldehyde to form a corresponding alcohol, i.e., the desired reaction, and the formation of heavy products, i.e., the undesired reactions. The major heavy products are dimers and trimers formed from aldol condensation of aldehydes and condensation of aldehyde with alcocol. The detailed product composition and reaction networks were discussed in reference [22]. We have also shown that NO and CO_2 could be used as molecules to probe the active sites that promote the hydrogenation and heavy product formation reactions, respectively, as the alcohol formation is correlated to CUS density while the heavy product formation can best be explained by the surface concentration of OH and possibly SH groups.

In this article, we present the results of our studies in which the effect of catalyst pre-treatment conditions on active site density and, in turn, on catalyst performance in aldehyde hydrogenation reactions was examined. The pre-treatment conditions examined are the sulfidation temperature and the post-sulfidation degassing temperatures. It appears that both of these parameters have a strong effect in determining the surface density of various active sites over the sulfided Ni–Mo/γ-Al_2O_3 catalysts. Catalysts that have been exposed to different pre-treatment conditions have been characterized using in situ X-ray diffraction (XRD), X-ray photoelectron spectroscopy (XPS), diffuse reflectance Fourier transform infrared spectroscopy (DRIFTS), temperature programmed desorption (TPD) and volumetric chemisorption measurement techniques. Catalyst performance with regard to activity and product distribution has been studied using two different linear aldehydes, hexanal and propanal.

2. Experimental

2.1. Catalyst preparation

Alumina-supported catalysts with different Mo and Ni loadings were prepared by wet co-impregnation of γ-Al_2O_3 with aqueous solutions of ammonium heptamolybdate and nickel nitrate. The preparation procedure was presented previously [20,23,24]. The catalyst compositions are reported as weight percentages of the oxide precursors, i.e., MoO_3 and NiO, following the convention commonly used in literature. The surface area of oxidic samples used in these studies varied between 166 and 195 m^2/g. Prior to reaction studies, the catalysts were sulfided in situ with 10% H_2S in H_2 for 10 h followed by degassing under a He flow for 2 h at the same temperature before cooling the catalyst bed to the desired reaction temperature. The standard sulfidation temperature was 400 °C except for those experiments where the sulfidation temperature was varied in the 300–600 °C range. The effect of He degassing treatment was examined by varying the degassing temperature in the range of 400–700 °C over catalysts that were sulfided at 400 °C.

XRD and XPS analyses on sulfided catalysts were done without exposing samples to the atmosphere. Catalysts were flushed with He at 400 °C for 2 h after sulfidation in reactor and then cooled to room temperature under He flow. The samples were then sealed using the valves located at both ends of the reactor tube and transferred to the sample chamber without exposure to air.

2.2. Catalyst characterization

2.2.1. XRD studies

X-ray powder diffraction (XRD) patterns were acquired by a Bruker D8 Advance X-Ray diffractometer equipped with atmosphere- and temperature-control capabilities (cryogenic to 1200 °C) and operated at 40 kV and 50 mA. The powder diffraction patterns were recorded in the 2θ range from 20 to 80°. In situ XRD of sulfided catalysts during reduction was performed under 5% H_2/N_2 gas flow stream using a linear temperature-program between isothermal steps. The catalysts were kept at isothermal steps for 0.5 h and the ramp rate in between the isothermal steps was 10 °C/min.

2.2.2. XPS studies

X-ray photoelectron spectroscopy analysis (XPS) was performed using an AXIS Ultra XPS spectrometer, operated at 13 kV and 10 mA with monochromator Al Kα radiation (1486.6 eV). Reduced and sulfided catalysts were mounted on sample holder with conductive tape in dry glove box filled with Ar. The sample holder was then transferred to the analysis chamber of the spectrometer with a controlled-atmosphere transporter. Charge neutralization was used to reduce effect of charge build-up on samples. All binding energies were referenced to Al 2p of 74.4 eV.

2.2.3. DRIFTS studies

Diffuse reflectance infrared Fourier transform spectroscopy (DRIFTS) experiments were performed using a Bruker IFS66 instrument equipped with DTGS and MCT detectors and KBr beam splitters. Catalyst was placed in a sample cup inside a Spectratech diffuse reflectance cell equipped with KBr windows and a thermocouple mount that allowed direct measurement of the surface temperature. Spectra for each experiment were averaged over 1000 scans in the mid-IR range (400–4000 cm^{-1}) to a nominal 3 cm^{-1} resolution.

The samples were sulfided in a reactor, which had two isolation valves on each end to allow its removal from the reaction system and air-free transfer for sulfided-sample characterization. Sulfided samples were transferred into DRIFTS cell in a glove box filled with Ar and the cell was isolated. After in situ pre-treatment of the samples with He at the desired temperature for 1 h, the temperature was decreased to the adsorption temperature used for different experiments and the background spectra were taken under He flow. NO and CO_2 adsorption process was carried out by introducing NO (5450 ppm in He) or CO_2 into the system at room temperature for 1 h. After adsorption, the system was subsequently purged for 1 h with He at a flow rate of 30 cm^3/min. The spectra were collected under He flow and the background spectrum was subtracted from the post-adsorption spectra. Pyridine was introduced through a diffusion tube for 20 min with He as the carrier gas, followed by flushing with He for 1.0 h. The spectra were collected with an MCT detector, which was operated at −196 °C.

2.2.4. Volumetric measurement

The volumetric measurements of CO_2 and NO chemisorption were performed using Micromeritics ASAP2010 instrument. Before chemisorption measurements, the catalysts were pre-treated in situ at the same conditions used prior to reaction experiments. Volumetric measurement involved plotting an adsorption isotherm, which showed the amount of gas adsorbed as a function of pressure. After completing the first adsorption measurement, the system was evacuated for 1 h at 10^{-5} Torr and a second adsorption isotherm was obtained. The amount of probe molecule chemisorbed was determined by taking the difference between the two isothermal adsorption measurements.

2.2.5. TPD studies

TPD experiments were performed using a system previously described [25]. The reactor effluent composition was continuously monitored as a function of sample temperature by a mass spectrometer (Hewlett-Packard, MS Engine 5898A). For each of the TPD runs, 200 mg of sample was loaded in the U-tube quartz reactor. All samples were sulfided in situ using the same procedure as in reaction studies, i.e., flowing 10% H_2S in H_2 for 10 h at 400 °C, followed He flushing for 1 h at the designated temperature and cooled down to 30 °C in He flow. Propanal adsorption was performed at 30 °C for 1.5 h by introducing propanal through a diffusion tube using a 30 cm^3 (STP)/min He flow at room temperature. After being flushed with He for 2 h at the same temperature, the samples were heated at a rate of 10 °C/min under a 30 cm^3 (STP)/min He flow.

2.3. Reaction studies

The reaction studies of hexanal and propanal hydrogenation were carried out in a fixed-bed reactor system, which is described in previous articles [20,21].

3. Results and discussion

3.1. XRD patterns of sulfided catalysts

Fig. 1 presents the X-ray diffraction patterns of 3% Ni–15% Mo/γ-Al_2O_3 samples sulfided at 300, 400, 500, and 600 °C. The diffraction patterns are obtained without exposing the samples to air following sulfidation. For comparison, the XRD pattern of the oxidized sample is also included. The pattern obtained over the oxide sample shows the primary diffraction lines from γ-Al_2O_3, with d-spacings of 1.40 Å (4 4 0), 1.98 Å (4 0 0), and 2.33 Å (3 1 1). As reported earlier [20], there is no evidence of crystalline MoO_3 at this loading level. There is also an additional feature, which may be due to $NiMoO_4$ (hkl = 2 2 0) at a d-spacing of 3.35 Å (JCPDS 45-0142). Instead, we start observing the diffraction lines that correspond to MoS_2 (hkl = 1 0 0, 1 0 2, 1 1 0, 1 1 2) at the d-spacings of 2.72, 2.49, 1.57, and 1.52 Å, respectively (JCPDS 75-1539), after sulfidation at 400 °C. The intensity of these diffraction lines increases with increasing sulfidation temperature. Another observation about these diffraction patterns is that, at sulfidation temperatures of 500 °C and above, additional phases appear, including a $NiSO_4$ phase (hkl = 1 1 1, 1 1 2, 1 3 0 with d-spacings of 3.56, 2.55, 2.33 Å, respectively, JCPDS 45-0142). There are additional diffraction lines in that region (d-spacings of 3.05, 2.09, and 1.79 Å) that coincide with those of Ni–Mo alloy or a nonstoichiometric phase $Ni_xMo_yS_z$, but an exact phase identification is not possible with the techniques used in this study.

Fig. 2 shows the X-ray diffraction patterns of the calcined and sulfided samples with different Mo loading levels. While the presence of crystalline MoO_3 does not appear over the oxide sample until a loading level of 15% MoO_3 is reached, the presence of MoS_2 is apparent even for loading

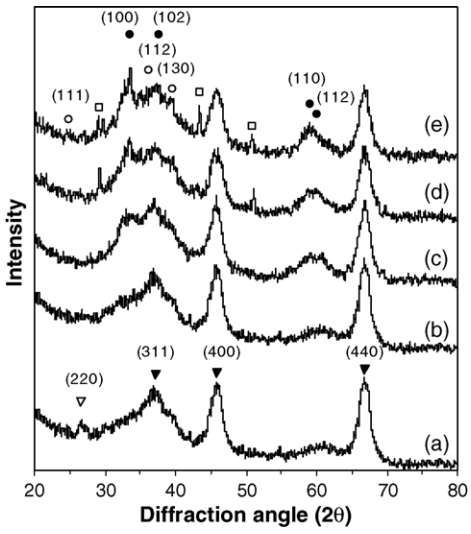

Fig. 1. X-ray diffraction patterns of 3% NiO–15% MoO_3/γ-Al_2O_3. (a) Calcined at 500 °C, (b) sulfided at 300 °C, (c) sulfided at 400 °C, (d) sulfided at 500 °C and (e) sulfided at 600 °C. (▼) Al_2O_3, (▽) $NiMoO_4$, (●) MoS_2, (◯) $NiMoS_4$ and (□) Ni–Mo alloy/$Ni_xMo_yS_z$.

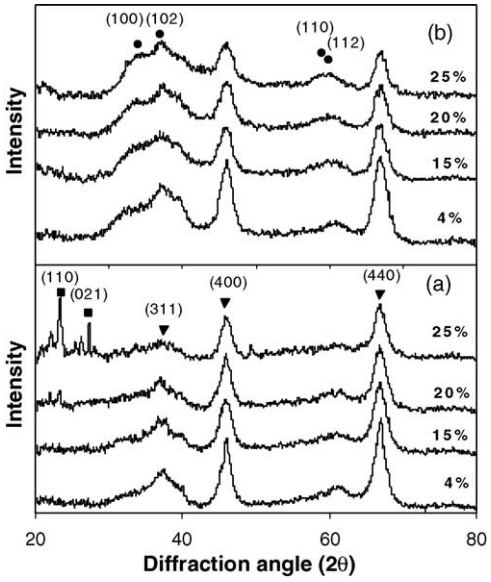

Fig. 2. X-ray diffraction patterns of calcined and sulfided MoO_3/γ-Al_2O_3 samples with different MoO_3 loading levels. (a) Calcined at 500 °C and (b) sulfided at 400 °C. (▼) Al_2O_3, (●) MoS_2 and (■) MoO_3.

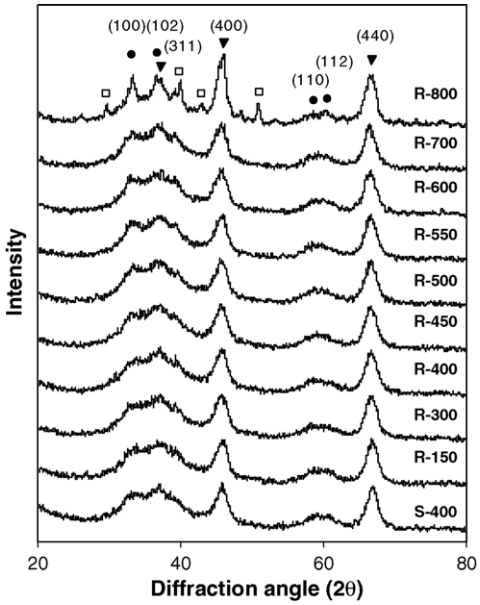

Fig. 3. In situ X-ray diffraction patterns of sulfided 3% Ni–15% Mo/γ-Al_2O_3 during temperature programmed reduction. (▼) Al_2O_3, (●) MoS_2, (□) Ni–Mo alloy/$Ni_xMo_yS_z$.

levels as low as 4%. This is consistent with our earlier results [20–22] where exposed alumina surface increased upon sulfidation, indicating a rearrangement of mono-layer molybdena species into the multi-layer structures of MoS_2 slabs. It should also be noted that the crystalline MoO_3, which is very apparent at 20 and 25% loading levels disappears upon sulfidation, indicating that the presence of crystalline MoO_3 does not hinder the sulfidation process. In fact, Li and Hercules [26] have reported the octahedrally coordinated three-dimensional species to sulfide more easily compared to the surface-coordinated tetrahedral species. The formation of MoS_2 slabs with hexagonal symmetry has been verified by various techniques in the literature, including HRTEM [27,28] and laser Raman spectroscopy [29–31], although their presence has not always been detected by X-ray diffraction [26]. It is possible that exposure of the samples to air after sulfidation could cause a partial re-oxidation and hence making it more difficult to observe the presence of MoS_2.

3.2. *In situ XRD of sulfided 3% Ni–15% Mo/γ-Al_2O_3 catalysts during reduction*

Fig. 3 shows the X-ray diffraction patterns obtained using the control-atmosphere analysis capability of the XRD system. X-ray diffraction patterns are taken in situ during a step-wise temperature-programmed reduction process of a sample which was sulfided at 400 °C. With increasing temperature below 400 °C, the intensity of the diffraction lines that are attributed to MoS_2 does not change significantly. These lines do not disappear even after reduction at 700 °C. This is consistent with our earlier temperature-programmed reduction (TPR) experiments where the H_2S elution from the sample was monitored by a mass spectrometer while the catalyst went through a linear temperature program under a 10% H_2 flow [14]. In those experiments, the decomposition of the MoS_2 phase was not complete until a much higher temperature (∼950 °C) was reached. This also explains why no metallic Ni or Mo phases appear in the in situ XRD experiment. Another point to note about the XRD patterns taken above 450 °C is that, the intensity of the diffraction lines that correspond to MoS_2 increased with increasing temperature. This may suggest an increase in the crystallinity of the MoS_2 phase, resulting in "thicker" slab sizes. At temperatures above 700 °C, there appears to be some Ni–Mo alloy or a nonstoichiometric phase $Ni_xMo_yS_z$ formation, however, the exact phase could not be identified.

3.3. *XPS of Mo–Ni/γ-Al_2O_3 catalysts sulfided at different temperatures*

Fig. 4 shows the Mo 3d-S 2s region of the X-ray photoelectron spectra of 3% Ni–15% Mo/γ-Al_2O_3 catalysts sulfided at 300, 400, 500, and 600 °C (S-300, S-400, S-500, S-600). The spectrum obtained over the pre-sulfidation sample (O-500), which has been calcined at 500 °C is also included. The deconvolution results of the spectrum for the sample sulfided at 300 °C clearly show three different oxidation states of Mo (IV, V, VI), indicating that the sulfidation process is not complete and the catalyst is in an 'oxy-sulfide' phase. The quantitative results based on the deconvoluted spectra, show the percentages of the Mo species in the (IV), (V), and (VI) oxidation states to be 48, 23, and 29%, respectively. S 2s region shows a signal, at 226 eV, suggesting that there is some partial sulfidation that has taken place. The spectrum of the sample sulfided at 400 °C shows that the sulfidation is close

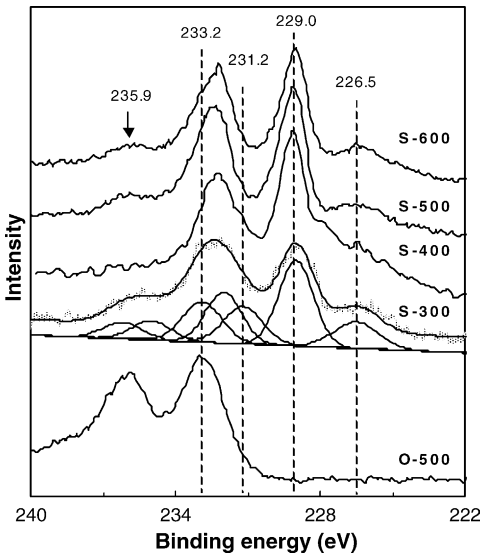

Fig. 4. X-ray photoelectron spectra (Mo 3d-S 2s region) of calcined and sulfided 3% NiO–15% MoO_3/γ-Al_2O_3 samples.

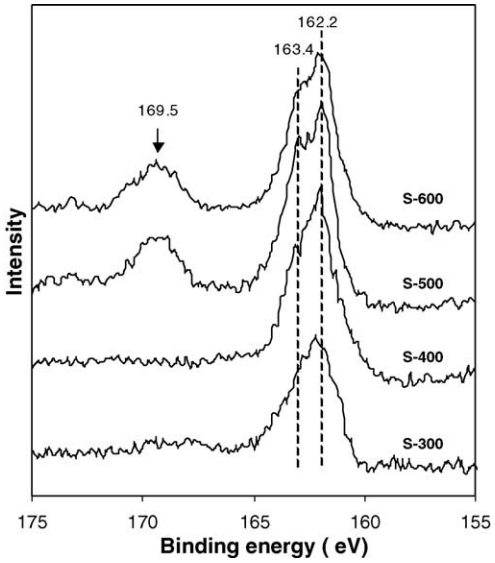

Fig. 6. X-ray photoelectron spectra (S 2p region) of sulfided 3% Ni–15% Mo/γ-Al_2O_3 samples.

to being complete, with IV being the primary oxidation state of Mo. The shoulder at 226 eV is also quite visible, showing the presence of a sulfide phase. The samples sulfided at higher temperatures, on the other hand, show a band around 235.9 eV and a clear shoulder around 233.2 eV.

Fig. 5 presents the Ni 2p region of the X-ray photoelectron spectra taken over the same set of samples. The spectrum obtained from the calcined sample shows Ni to be in a nickel oxide phase, with a $2p_{3/2}$ binding energy of 856.5 eV. After sulfidation at 300 °C, there appears to be two different oxidation states, one corresponding to an oxide phase (about 49%) and one corresponding to a sulfide phase (about 51%), typical of a NiMoS structure ($2p_{3/2}$ at 853.4 eV). Sulfiding

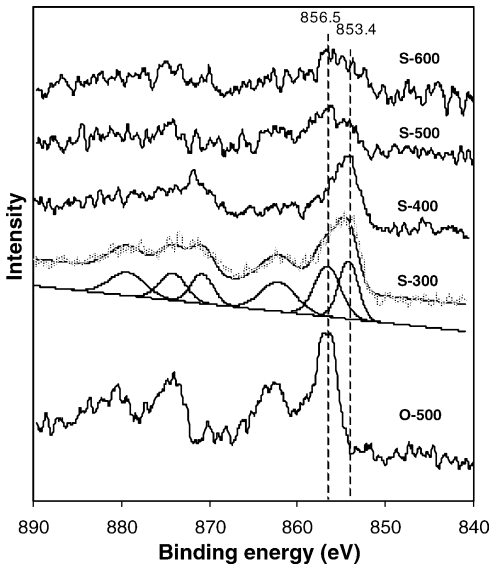

Fig. 5. X-ray photoelectron spectra (Ni 2p region) of calcined and sulfided 3% NiO–15% MoO_3/γ-Al_2O_3 samples.

at 400 °C appears to be sufficient to complete the sulfidation of the "sulfidable" Ni sites (∼75% of total Ni species). As reported previously [32], the other ∼25% Ni species exist in a $NiAl_2O_4$ matrix, which cannot be sulfided or reduced. Sulfidation at higher temperatures, gives rise to the appearance of two different binding energies, the higher one possibly corresponding to a sulfate species ($NiSO_4$) [33].

The S 2p region of the X-ray photoelectron spectra is presented in Fig. 6. The separation between the S $2p_{1/2}$ and S $2p_{3/2}$ binding energies is very small (∼1.18 eV), which makes it difficult to deconvolute the S 2p spectra. The sample sulfided at 300 °C shows a broad feature in the 162–163 eV range. This band becomes more intense after sulfidation at 400 °C. What is interesting about the spectra taken over samples sulfided at higher temperatures is the appearance of a band centered at 169.5 eV. This binding energy, which was not observed over samples sulfided at lower temperatures, corresponds to a sulfate species. At this point, it is not possible to determine conclusively whether the sulfate species are affiliated with Mo or Ni centers or both. The feature observed around 235.9 eV in the Mo 3d spectrum (Fig. 4) of the samples that were sulfided at higher temperatures may be due to some of the Mo sites "oxidizing" to a higher oxidation state, such as $Mo(SO_4)_3$. It is also possible that this peak may be due to the binding energy of a S 2s electron in a sulfate group, as suggested by Friedman et al. [34].

Since the Al 2p region of the spectra (not shown) taken over samples sulfided at different temperatures does not change much with sulfidation temperature, an involvement from the Al species is not very likely. However, formation of a $NiSO_4$ phase remains as a distinct possibility. A similar conclusion was reached by Delmon and co-workers about the formation of a $CoSO_4$ phase in a Co–Mo/Al_2O_3 catalyst [35]. The O 1s region of the spectra taken over the same samples

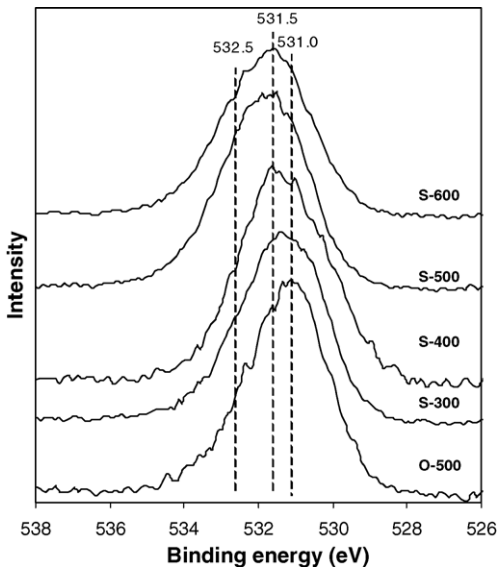

Fig. 7. X-ray photoelectron spectra (O 1s region) of calcined and sulfided 3% Ni–15% Mo/γ-Al_2O_3 samples.

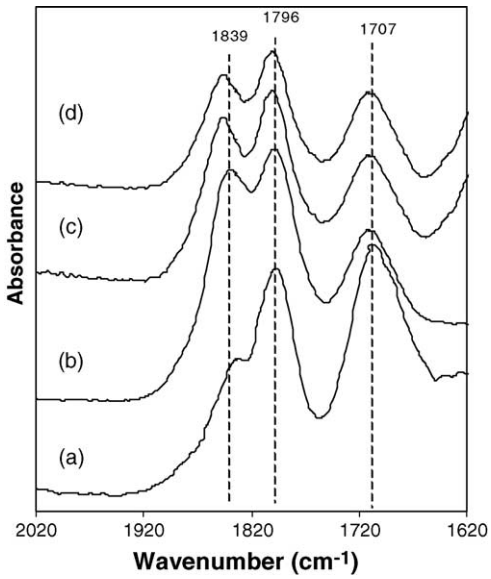

Fig. 8. DRIFTS Spectra of NO adsorbed on 3% Ni–15% Mo/Al_2O_3 catalysts sulfided at (a) 300, (b) 400, (c) 500, and (d) 600 °C.

is presented in Fig. 7. For the oxidized sample, the band is centered around 531.0 eV and has contributions from MoO_3 and NiO. Since the oxidized sample is close to a mono-layer coverage [20,21], the contribution from the alumina surface is not very noticeable. With increasing sulfidation temperature, the peak shifts to higher binding energies and becomes less symmetrical. Since sulfidation decreases the surface coverage and leads to higher alumina exposure, the shift observed in the O 1s peak may be due to an increased contribution from Al_2O_3 (531.5 eV). The shoulder that appears around 532.5 eV at higher sulfidation temperatures can be explained by the formation of sulfate species, since O 1s binding energy in $NiSO_4$ is reported to be around 532.5 eV [36]. It is conceivable that OH groups left on the surface after sulfidation serve as oxygen sources in the formation of the sulfate species. DRIFTS results, which have shown OH groups to exist over catalysts sulfided at 500 °C and the "blank" TPD profiles over sulfided catalysts, which have shown water desorption at temperatures as high as 600–700 °C, support this assertion.

The results obtained from XPS are complementary to the XRD data in showing that it is necessary to sulfide the catalysts at 400 °C to achieve complete sulfidation, and that higher sulfidation temperatures lead to the formation of additional phases.

3.4. DRIFTS of adsorbed NO, CO_2, and pyridine molecules

3.4.1. NO and CO_2 adsorption

Fig. 8 shows the DRIFT spectra taken following NO adsorption over 3% Ni–15% Mo/γ-Al_2O_3 samples sulfided at different temperatures. Two strong bands that correspond to stretching vibrations of N=O adsorbed on Mo sites (1707 and 1796 cm^{-1}) are observed after sulfidation at 300 °C. The NO bands from Ni-associated sulfur vacancies (1839 cm^{-1}), on the other hand, are weak at this temperature. This observation is in agreement with our earlier findings where the TPR experiments of sulfided catalysts were shown to form Mo-associated sulfur vacancies at lower temperatures, comparing the formation of Ni-associated S-vacancies [14]. The bands associated with Mo centers decrease in intensity as sulfidation temperature increase from 300 to 400 °C while intensity of the bands associated with Ni centers grows significantly, suggesting that some of the surface Mo centers are being "replaced" or taken up by Ni sites. Sulfidation at temperatures above 400 °C appears to decrease the sulfur vacancies associated with Ni sites. This could be due to sintering of Ni–Mo-S slabs or/and Ni–Mo alloy formation as well. However, loss of Ni sites due to the formation of a sulfate phase, as seen in XPS results, cannot be ruled out.

Fig. 9 shows the DRIFT spectra taken following NO adsorption over samples that are sulfided at 400 °C, but degassed with He at different temperatures. The intensity of the bands associated with Mo sites increases as degassing temperature is increased from 400 to 600 °C. As seen in our H_2S TPD experiments over sulfided catalysts [14], where association of SH groups and H^+ ions from Brønsted acid sites and desorption of H_2S were observed in the 400–600 °C range, heating the catalyst under He at these temperatures creates more S vacancies, and hence more NO adsorption sites. The intensity of the NO bands associated with Ni sites appears to be insensitive to the flushing temperature. This is also consistent with earlier findings from the literature where Brønsted acid sites are concluded to be mainly associated with Mo centers, using evidence based on TPD [14] and IR spectroscopy of pyridine adsorption results [37]. Further increases in temperature, however, may result in sintering of MoS_2 crystallites, as

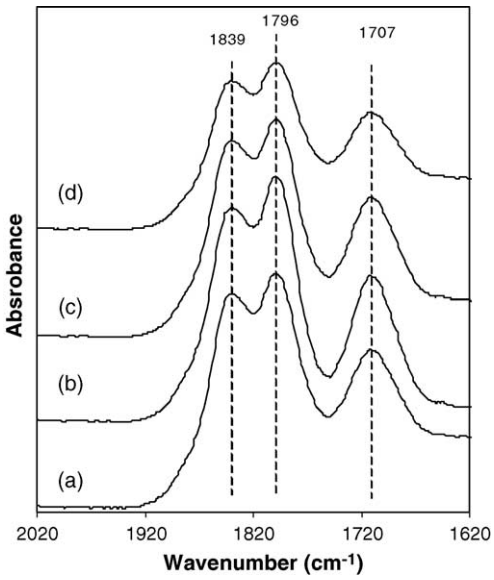

Fig. 9. DRIFTS Spectra of NO adsorbed on sulfided 3% Ni–15% Mo/Al_2O_3 catalysts degassed with He at (a) 400, (b) 500, (c) 600, and (d) 700 °C.

observed by the decrease in the intensity of 1707 cm^{-1} band. The band associated with the Ni sites (1839 cm^{-1}) also decreases somewhat, possibly because sintering of MoS_2 slabs can reduce the edge planes where Ni sites are located.

3.4.2. Pyridine adsorption

Fig. 10 shows the adsorbed pyridine bands (adsorbed at 150 °C followed by flushing with He at the same temperature) over samples that are sulfided at 400 °C, but degassed with He at different temperatures. A detailed discussion of the band assignments of adsorbed pyridine over oxidized, sulfided, and reduced Ni–Mo catalysts was presented in our previous article [32]. The sulfided (400 °C) sample following degassing with He at the same temperature (400 °C) shows strong bands arising (1445, 1575 cm^{-1}) from pyridine adsorbed on Lewis acid sites along with relatively weak bands (1538 and 1635 cm^{-1}) from pyridine adsorbed on Brønsted acid sites. With increasing degassing temperature, intensity of the bands associated with L sites grows gradually, while the intensity of the bands associated with B sites decreases and disappears above 500 °C. This finding is consistent with NO adsorption DRIFTS results (Fig. 9), which showed an increase in the NO bands adsorbed on Mo-associated CUS. Higher degassing temperatures result in association of SH groups and H^+ ions from Brønsted acid sites and desorption of H_2S, leaving behind Mo-associated S vacancies. The increase in the intensity of pyridine adsorbed on L sites is also consistent with this observation since S vacancies are expected to have Lewis acid character. The increase in the Lewis acid sites could also result from the alumina support, which could go through "dehydration" at higher degassing temperatures, leading to the formation of additional L sites.

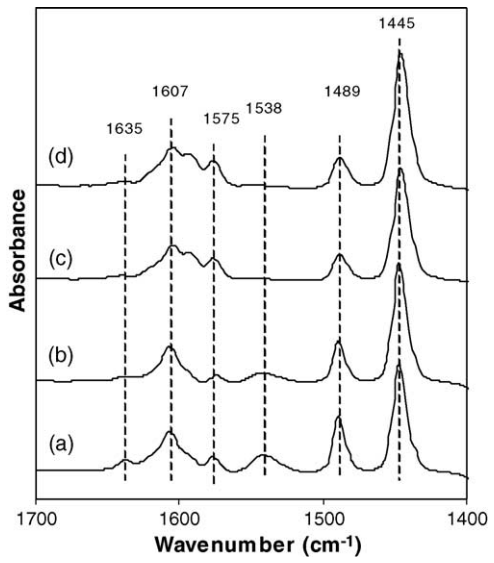

Fig. 10. DRIFTS spectra of pyridine adsorbed on sulfided 3% Ni–15% Mo/Al_2O_3 catalysts degassed with He at (a) 400, (b) 450, (c) 500, and (d) 600 °C.

3.5. Volumetric measurements for NO and CO_2 chemisorption

Fig. 11 shows the NO and CO_2 uptake as a function of sulfidation temperature over 3% Ni–15% MO/γ–Al_2O_3 catalyst. NO adsorption increases significantly with sulfidation temperature from 300 to 400 °C. It appears to plateau between 400 and 500 °C before it starts decreasing at higher sulfidation temperatures. These results are quite consistent with NO adsorption DRIFTS findings. CO_2 adsorption capacity also increases when sulfidation temperature is increased from 300 to 400 °C. This observation is in agreement with our earlier assertion that sulfidation increases the exposed alumina surface compared to the oxide samples due to Mo aggregation during the formation of the MoS_2 slabs [19,20]. The decrease observed in CO_2 uptake with increasing sulfidation tempera-

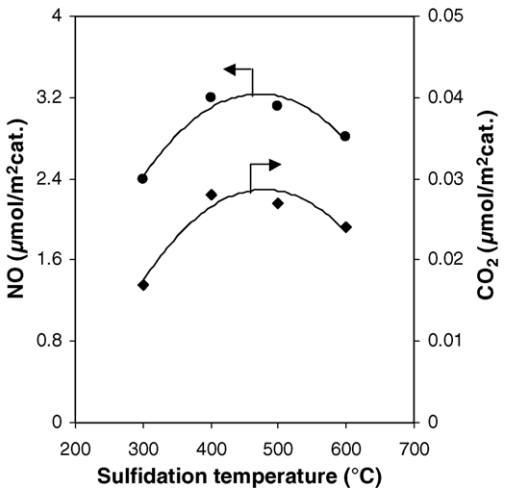

Fig. 11. Effect of sulfidation temperature on NO and CO_2 chemisorption capacities over sulfided 3% Ni–15% Mo/Al_2O_3 catalysts.

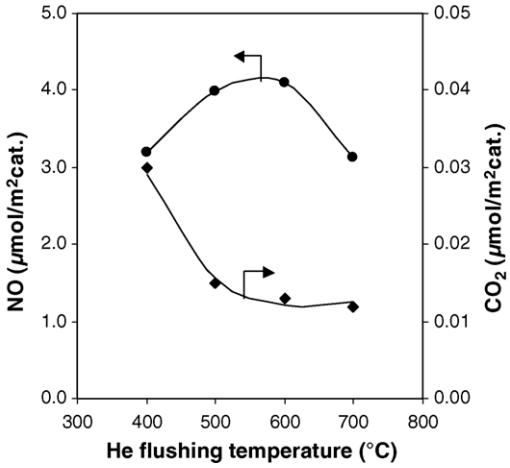

Fig. 12. Effect of post-sulfidation degassing temperature on NO and CO_2 chemisorption capacities over sulfided 3% Ni–15% Mo/Al_2O_3 catalysts.

tures is likely due to elimination of hydroxyl groups at higher temperatures.

Fig. 12 shows NO and CO_2 adsorption capacities over samples that are sulfided at 400 °C, but degassed with He at different temperatures. NO uptake goes through a maximum when the degassing temperature is kept between 500 and 600 °C. CO_2 uptake, on the other hand, decreases significantly with increasing degassing temperatures and reaches a plateau around 600 °C. The decrease in CO_2 uptake can again be explained with the dehydration of the support at elevated temperatures.

3.6. TPD profiles over sulfided catalysts

"Blank" TPD experiments were performed by exposing samples that were sulfided in situ to a linear temperature program under a He flow while the effluent stream was analyzed continuously by on-line mass spectrometry for desorbing species. Fig. 13 shows the H_2S and H_2O profiles obtained through a blank TPD experiment over a 3% Ni–15% Mo/Al_2O_3 catalyst. The H_2S signal, that arises around 400 °C and reaches a maximum at 500 °C, signals the loss of sulfhydryl groups from the surface and increase in anion vacancies, likely associated with Mo centers [38,39]. The importance of surface SH or sulfhydryl groups has been discussed with regard to several reaction mechanisms [14,18,40–43]. The evidence for the presence of SH groups has been provided by deuterium exchange studies [44], chemical titration by silver ions [40], Raman spectroscopy [31], and infrared spectroscopy [45]. The Brønsted acidity associated with SH groups in sulfided catalyst was also examined using IR spectroscopy of adsorbed pyridine species [36,37]. Some correlations between the HDS activity and SH concentration have been reported previously [46–50]. The effects of the changes in the surface concentration of Brønsted acid sites and sulfur vacancies on the hydrogenolysis and hydrogenation activities in HDN and HDO reactions have also been discussed [14,18]. The H_2O desorption profile from the same blank TPD experiment shows a broad maximum centered around 600 °C. This feature signals dehydration of the surface and hence loss of OH groups. The desorption behavior for H_2S and H_2O from the sample helps explain the changes observed in NO and CO_2 adsorption capacities with degassing temperature. The minimum observed for CO_2 uptake at a degassing temperature of 600 °C corresponds to the maximum seen in H_2O desorption profile since CO_2 serves as a probe for the surface OH groups. Similarly, the maximum NO adsorption capacity observed when the sample is degassed between 400 and 500 °C, corresponds to the maximum reached in the anion vacancies created since NO is a probe molecule for the sulfur vacancy sites.

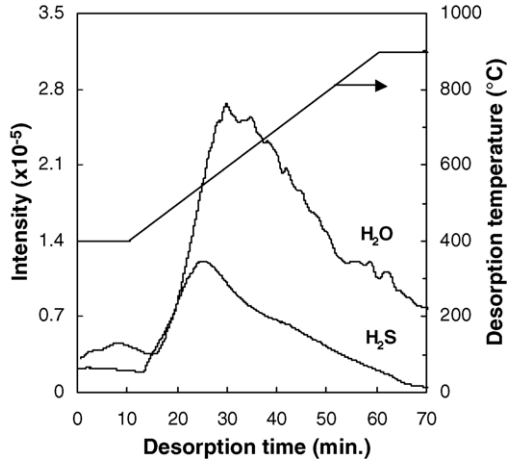

Fig. 13. Blank TPD profile of sulfided 3% Ni–15% Mo/Al_2O_3 catalyst.

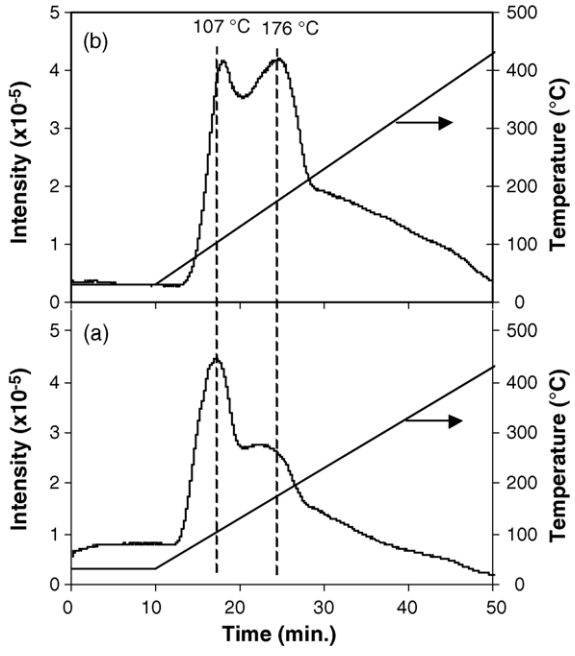

Fig. 14. Propanal TPD profiles over 3% Ni–15% Mo/Al_2O_3 samples sulfided at 400 °C and degassed with He at (a) 400 and (b) 500 °C.

Table 1
Effect of sulfidation temperature on catalyst performance in propanal hydrogenation (3% Ni–15% Mo/Al_2O_3)

Reaction[a]	Sulfidation[b]	C%-hexanal[c]	Y%-hexanol[c]	Y%-lights	Y%-heavies
140 °C	300	44.3	26.2	4.1	14.0
	400	61.0	38.8	0.7	21.5
	500	59.6	38.3	2.5	18.8
	600	53.2	31.1	4.0	18.1
160 °C	300	50.1	30.7	5.2	14.3
	400	71.0	47.5	1.3	22.2
	500	70.1	46.6	3.6	19.9
	600	65.5	40.5	5.3	19.7
180 °C	300	68.2	43.8	8.3	16.1
	400	87.0	61.8	1.8	23.4
	500	85.9	59.5	4.7	21.7
	600	82.6	52.9	8.4	21.3

[a] Reaction conditions: 0.56% propanal in 250 ml/min H_2 at 1000 psi.
[b] Sulfided in 10% H_2S in H_2, 10 h.
[c] C%-conversion, Y%-yield.

Propanal TPD profiles from two 3% Ni–15% Mo/Al_2O_3 samples sulfided at 400 °C, but degassed at two different temperatures are presented in Fig. 14. They are obtained by monitoring the $m/e = 29$ ion, which represents the desorbing propanal signal. Both samples show two main desorption features at about 107 and 176 °C. The main difference between the two samples is that the one degassed at a higher temperature following sulfidation, shows a higher intensity of the desorption feature at 176 °C and a lower intensity of the feature at 107 °C. This would suggest that propanal adsorption may be directly affected by the post-sulfidation degassing temperature. Based on our results presented above, it is conceivable that the higher-temperature desorption is from the coordinatively unsaturated sites (CUS) which increase with increasing degassing temperatures while the lower-temperature desorption is from hydroxyl and sulfhydryl groups which decrease when the sample is degassed at higher temperatures.

3.7. Aldehyde hydrogenation over sulfided 3% Ni–15% Mo/γ-Al_2O_3 catalysts

The effect of pre-treatment conditions on catalyst performance in aldehyde hydrogenation has been summarized in Tables 1–3. Table 1 presents the conversion and yield data from propanal hydrogenation over 3% Ni–15% Mo/Al_2O_3 catalysts for three different reaction temperatures to demonstrate the effect of sulfidation temperature on catalyst performance. The yield is defined as the percent of feed aldehyde converted to a given product. As expected, the catalyst sulfided at 300 °C, shows a much lower activity since sulfidation is not yet complete at that temperature. With increasing sulfidation temperature, both the conversion and the propanol yield increase and reach a plateau between 400 and 500 °C, corresponding to a maximum in the CUS surface density. Further increases in sulfidation temperatures lead to a loss of activity and propanol yield, as some of the active sites are

Table 2
Effect of post-sulfidation degassing temperature on catalyst performance in propanal hydrogenation (sulfided 3% Ni–15% Mo/Al_2O_3 catalyst[a])

Reaction[b]	Post-treatment[c]	C%-hexanal[d]	Y%-hexanol[d]	Y%-lights	Y%-heavies
140 °C	400	61.0	38.8	0.7	21.5
	500	64.2	50.0	1.4	12.8
	600	63.8	49.4	2.6	11.8
	700	49.8	34.1	4.6	11.1
160 °C	400	71.0	47.5	1.3	22.2
	500	76.5	60.9	1.9	13.7
	600	74.7	58.9	3.1	12.7
	700	60.6	42.4	6.4	11.8
180 °C	400	87.0	61.8	1.8	23.4
	500	93.6	76.9	2.2	14.5
	600	94.8	76.8	4.0	14.0
	700	79.3	56.1	9.4	13.8

[a] Sulfided at 400 °C in 10% H_2S in H_2, 10 h.
[b] Reaction conditions: 0.56% propanal in 250 ml/min H_2 at 1000 psi.
[c] Post-degassing with He for 2 h.
[d] C%-conversion, Y%-yield.

Table 3
Effect of post-sulfidation degassing temperature on catalyst performance in hexanal hydrogenation (sulfided 3% Ni–15% Mo/Al_2O_3 catalyst[a])

Reaction[b]	Pre-treatment[c]	C%-hexanal[d]	Y%-hexanol[d]	Y%-lights	Y%-heavies
140 °C	400	22.6	16.8	0.7	5.1
	500	26.2	22.0	0.8	3.4
	600	25.5	22.0	0.8	2.7
	700	18.2	14.8	0.7	2.7
160 °C	400	57.3	48.9	1.8	6.6
	500	65.5	59.4	2.2	4.1
	600	66.2	60.2	2.3	3.7
	700	50.1	44.5	2.2	3.4

[a] Sulfided at 400 °C in 10% H_2S in H_2, 10 h.
[b] Reaction conditions: 0.09% hexanal in 250 ml/min H_2 at 1000 psi.
[c] Post-degassing with He for 2 h.
[d] C%-conversion, Y%-yield.

lost due to sulfate formation as seen in the XPS analysis. It is interesting to note that the heavy product yield shows a substantial increase when sulfidation temperature is raised from 300 to 400 °C. If the heavy product formation is promoted primarily by the OH groups over exposed alumina surfaces, this result should be expected since the sulfidation causes an increase in the exposed alumina surfaces as the MoS_2 slabs are formed. As seen in the blank TPD experiments, above 400 °C, the dehydration of the surface takes place, decreasing the number of OH groups, and hence the heavy product yield.

Table 2 shows the effect of post-sulfidation degassing temperature on the propanal conversion and product yield. At all three reaction temperatures used, there is significant improvement in catalyst performance when the degassing temperature is raised from 400 to 500 °C. The improved performance is especially evident in increased hexanol yield and decreased heavy product yield. Increasing the degassing temperature to 600 °C does not lead to any significant changes in activity or product distribution although further increase in degassing temperature results in both activity and alcohol yield loss. The heavy product yield, on the other hand, does not appear to be much affected. The improved performance observed as the degassing temperature is increased from 400 to 500 °C likely due to an increase in anion vacancies accompanied by a decrease in hydroxyl and sulfhydyl groups on the surface. Much higher degassing temperatures, i.e., 700 °C, however, lead to increased growth in crystallite sizes, and hence to decreased activity.

The trends observed in the hexanal hydrogenation reactions are identical to those seen in propanal hydrogenation (Table 3). They are also consistent with the results of our NO and CO_2 adsorption experiments.

3.8. Correlation of adsorption sites and aldehyde hydrogenation performance over sulfided catalysts

NO and CO_2 adsorption sites were correlated with the aldehyde hydrogenation performance of catalysts sulfided and/or degassed at different temperatures using two different aldehyde molecules, propanal and hexanal. Fig. 15a shows

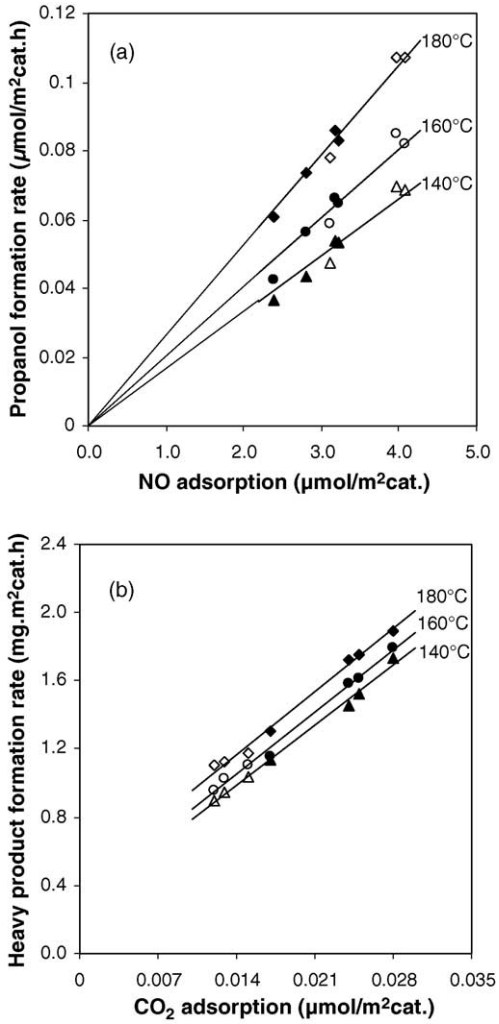

Fig. 15. Correlation of propanol formation rates and heavy product formation rates with NO (a) and CO_2 (b) adsorption capacities over 3% Ni–15% Mo/Al_2O_3 catalysts sulfided and/or degassed at different temperatures. (Solid points represent catalysts sulfided at different temperatures; blank points represent catalysts sulfided at 400 °C and degased with He at different temperatures.).

the propanol formation rate over a sulfided 3% Ni–15% Mo/Al_2O_3 catalyst as a function of NO adsorption capacity. Different symbols represent different reaction temperatures. As seen in the figure, the propanol formation rate increases linearly with NO adsorption capacity. This trend holds true for every reaction temperature tested. It is also interesting to note that all data points that represent different sulfidation temperatures and/or different degassing temperatures fall on a straight line, which approximately goes through the origin. The variation of heavy product formation rate in propanal hydrogenation with CO_2 adsorption capacity for the same set of catalyst samples is presented in Fig. 15b for three different reaction temperatures and samples that were sulfided and/or degassed at different temperatures. All of the results point to a linear correlation between heavy product formation rate and CO_2 uptake capacity of the catalysts. This result is consistent with earlier findings [20,21] where CO_2 was shown to be a proper probe molecule for the alumina hydroxyl sites, which in turn, were shown to catalyze the heavy product formation reactions. Unlike the correlation between propanol formation rate and NO uptake capacity, these straight lines do not seem to go through the origin, suggesting that there may be additional sites, such as SH groups over Mo centers, leading to heavy formation over these catalysts.

Fig. 16 shows hexanal hydrogenation data that show the correlation of hexanol formation rate and heavy product formation rate with NO and CO_2 uptake capacity, respectively. The data points represent different degassing temperatures. The linear relationship is once more evident in both cases, showing identical trends as those observed in propanal hydrogenation reactions.

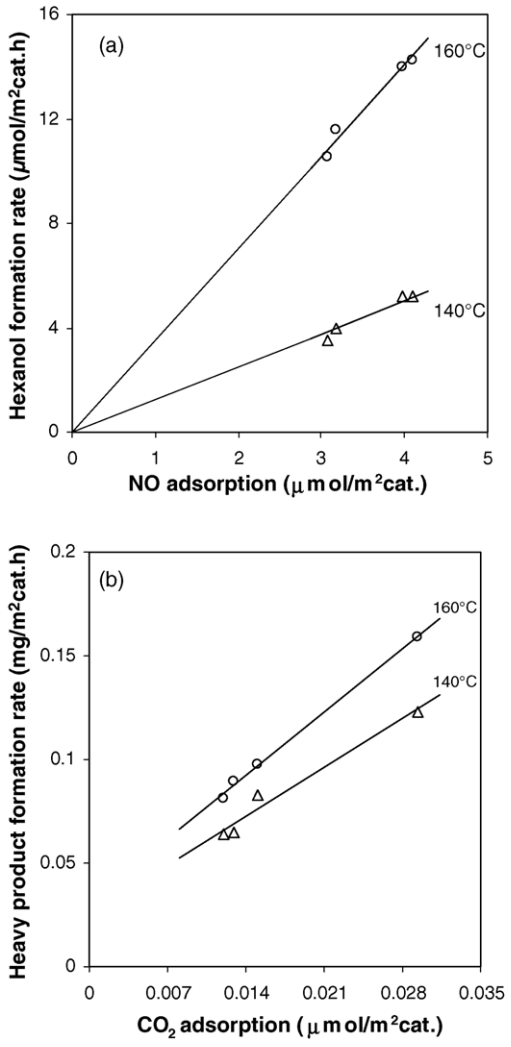

Fig. 16. Correlation of hexanol formation rates and heavy product formation rates with NO (a) and CO_2 (b) adsorption capacities over 3% Ni–15% Mo/Al_2O_3 catalysts degassed at different temperatures.

4. Summary

It appears that the pre-treatment conditions such as sulfidation temperature and post-sulfidation degassing temperatures can be effectively used to manipulate the surface density of anion vacancy sites and the hydroxyl and sulfhydryl sites over the sulfided Ni–Mo/Al_2O_3 catalysts. Any changes in the surface density of these sites, in turn, can have significant effect on the activity and product distribution achieved over these catalysts in hydrogenation of linear aldehydes. As established in our previous article [21], NO and CO_2 can be used to probe the sites that promote the alcohol and heavy product formation reactions, respectively. The results obtained from XRD, XPS, DRIFTS and volumetric chemisorption measurements provide complementary information in establishing the correlations between the active sites and reaction performance.

References

[1] H. Topsøe, B.S. Clausen, Catal. Rev. Sic. Eng. 26 (1984) 395.
[2] H. Topsøe, B.S. Clausen, R. Candia, C. Wivel, S. Morup, J. Catal. 68 (1981) 433.
[3] C. Wivel, R. Candia, B.S. Clausen, S. Morup, H. Topsøe, J. Catal. 87 (1984) 497.
[4] H. Topsøe, B.S. Clausen, Appl. Catal. 25 (1986) 273.
[5] N-Y. Topsøe, H. Topsøe, J. Catal. 84 (1983) 386.
[6] H. Topsøe, B.S. Clausen, F.E. Massoth, in: J.R. Anderson, M. Boudart (Eds.), Science and Technology, vol. 11, Springer-Verlag, Berlin, 1996.
[7] T.C. Ho, Catal. Rev. Sci. Eng. 30 (1988) 117.
[8] C.N. Satterfield, Heterogeneous Catalysis in Industrial Practice, Second ed., McGraw-Hill, New York, 1991, p. 383, Chapter 9.
[9] M.J. Girgis, B.C. Gates, Ind. Eng. Chem. Res. 30 (1991) 2021.
[10] G. Perot, Catal. Today 10 (1991) 447.
[11] E. Laurent, B. Delmont, J. Catal. 146 (1994) 281.
[12] R. Prins, Hydrodesulfurizayion, hydrodenitrogenation, hydrodeoxygenation, and hydrodechlorination, in: G. Ertl, H. Knozinger, J. Weitkamp (Eds.), Handbook of Heterogeneous Catalysis, VCH, 1997.
[13] S.C. Kim, F.E. Massoth, Ind. Ehg. Chem. Res. 39 (2000) 1705.
[14] L. Zhang, G. Karakas, U.S. Ozkan, J. Catal. 178 (1998) 457.

[15] A. Bunch, L. Zhang, G. Karakas, U.S. Ozkan, Appl. Catal. 190 (2000) 51.
[16] E. Furimsky, Appl. Catal. 6 (1983) 159.
[17] M.W. Vogelzang, C.L. Li, G.A. Schuit, B.C. Gates, L. Petrakis, J. Catal. 84 (1983) 170.
[18] A.Y. Bunch, U.S. Ozkan, J. Catal. 206 (2002) 177.
[19] J.J. MeKetta, W.A. Cunningham, Encyclopedia of Chemical Processing and Design, 33, New Yorkand Basel, 1990, p. 46.
[20] X. Wang, G. Li, U.S. Ozkan, J. Mol. Catal. 217 (2004) 219.
[21] X. Wang, U.S. Ozkan, J. Catal. 227 (2004) 492.
[22] X. Wang, R.Y. Soleh, U.S. Ozkan, in press.
[23] U.S. Ozkan, S. Ni, L. Zhang, E. Moctezuma, Energy Fuels 8 (1994) 249.
[24] U.S. Ozkan, L. Zhang, S. Ni, E. Moctezuma, J. Catal. 148 (1994) 181.
[25] U.S. Ozkan, Y. Cai, M.W. Kumthekar, L. Zhang, J. Catal. 142 (1993) 182.
[26] C.P. Li, D.M. Hercules, J. Phys. Chem. 88 (1984) 456.
[27] F. Delannay, P. Gajardo, P. Grange, B. Delmon, J. Chem. Soc. Faraday Trans. I 76 (1980) 988.
[28] R.M. Stockmann, H.W. Zandbergen, A.D. van Langeveld, J.A. Moulijin, J. Mol. Catal. 102 (1995) 147.
[29] F.R. Brown, L.E. Makovsky, Appl. Spectosc. 31 (1977) 44.
[30] G. Schrader, C.P. Cheng, J. Catal. 80 (1983) 369.
[31] E. Payen, S. Kasztelan, J. Grimblot, J. Mol. Structure 174 (1988) 71.
[32] X. Wang, U.S. Ozkan, J. Phys. Chem. B, in press.
[33] D.L. Legrand, H.W. Nesbitt, G.M. Bancroft, Am. Mineral. 83 (1998) 1256.
[34] R.M. Friedman, R.I. Declerck-Grimee, J.J. Fripiat, J. Electr. Specrosc. Related Phenom. 5 (1974) 437.
[35] L. Portela, P. Grange, B. Delmon, J. Catal. 156 (1995) 243.
[36] J.F. Moulder, W.F. Stickle, P.E. Sobol, K.D. Bomben, in: J. Chastain (Ed.), Handbook of X-ray Photoelectron Spectroscopy, Perkin–Elmer Corporation, Minnesota, 1992.
[37] N-Y. Topsøe, H. Topsøe, F.E. Massoth, J. Catal. 119 (1989) 252.
[38] G.C.A. Schuit, Int. J. Quantum Chem. 12 (Suppl. 2) (1977) 43.
[39] C.J. Wright, C. Sampson, D. Fraster, R.B. Moyes, P.B. Wells, C. Riekel, J. Chem. Soc. Faraday Trans. I 76 (1980) 1585.
[40] A.M. Escudey-Castro, L. Broussiers McLeeod, E.J. Gil-Llambias, Appl. Catal. 4 (1982) 371.
[41] F.E. S Massoth, Proceedings of the Fourth International Conference, The Chemistry and Uses of Molybdenum, Golden, Colorado, 1982.
[42] J. Maternova, Appl. Catal. 3 (1982) 3.
[43] G. Muralidhar, F.E. Massoth, J. Shabtai, J. Catal. 85 (1984) 44.
[44] F.E. Massoth, J. Catal. 36 (1975) 164.
[45] N-Y. Topsøe, H. Topsøe, J. Catal. 139 (1993) 641.
[46] S.H. Yang, C.N. Satterfield, J. Catal. 81 (1983) 168.
[47] J. Maternova, Appl. Catal. 6 (1982) 61.
[48] V. Stuchly, L. Baranek, Appl. Catal. 35 (1987) 35.
[49] L. Vivier, G. Kasztelan, Perot, Bull. Soc. Chim. Belg. 100 (1991) 801.
[50] J. Miciukiewicz, W. Zmierczak, F.E. Massoth, Bull. Soc. Chim. Belg. 96 (1987) 915.